VERSITA

Acta Geophysica
DOI: 10.2478/s11600-013-0121-5

Regional Ionosphere Modeling in Support of IRI and Wavelet Using GPS Observations

Yazdan AMERIAN, Behzad VOOSOGHI,
and Masoud M. HOSSAINALI

Faculty of Geodesy and Geomatics Engineering,
K.N. Toosi University of Technology, Tehran, Iran
e-mails: amerian@dena.kntu.ac.ir (corresponding author),
vosoghi@kntu.ac.ir, hossainali@kntu.ac.ir

Abstract

Dual-frequency global navigation satellite systems (GNSS) observations provide most of the input data for development of global ionosphere map (GIM) of vertical total electron content (VTEC). The international GNSS service (IGS) develops different ionosphere products. The IGS tracking network stations are not homogeneously distributed around the world. The large gaps of this network in Middle East, *e.g.*, Iran plateau, reduce the accuracy of the IGS GIMs over this region. Empirical ionosphere models, such as international reference ionosphere (IRI), also provide coarse forecasts of the VTEC values. This paper presents a new regional VTEC model based on the IRI 2007 and global positioning system (GPS) observations from Iranian Permanent GPS Network. The model consists of a given reference part from IRI model and an unknown correction term. Compactly supported base functions are more appropriate than spherical harmonics in regional ionosphere modeling. Therefore, an unknown correction term was expanded in terms of B-spline functions. The obtained results are validated through comparison with the observed VTEC derived from GPS observations.

Key words: compactly supported base functions, global ionosphere map, global positioning system, international reference ionosphere, total electron content.

1. INTRODUCTION

During the last decades, global positioning satellite system (GPS) has become a common tool for analyzing the Earth's atmosphere. The ionosphere is the upper most part of the atmosphere which is extended from about 60 to 2000 km. In this layer of ionosphere, the density of free electrons is large enough to significantly affect the propagation of electromagnetic waves. The resulting signal delay is inversely proportional to the square of the signal frequency. Slant total electron content (STEC), the linear integral of the electron density along the propagation path of an electromagnetic wave from satellite to receiver, and the electron density provide valuable information as to the ongoing physical processes in this part of atmosphere (Liu and Gao 2003). GPS and other global navigation satellite systems (GNSS) broadcast signals on two or more frequencies which can be used to measure the ionospheric delay. Computed delays are used for modeling the electron density or STEC (Hernandez-Pajares *et al.* 1999).

The Ionosphere Working Group of the International GNSS Service (IGS), including Centre for Orbit Determination in Europe (CODE), European Space Agency (ESA), Jet Propulsion Laboratory (JPL), and Universidad Politecnica de Cataluna (UPC), delivers daily global ionosphere maps (GIM) of vertical total electron content (VTEC) in the IONospheric EXchange (IONEX) format since 1998 by using different estimation methods (Hernandez-Pajares *et al.* 2009). The IGS combined GIM is also delivered from 2005. The GNSS data of three successive days is usually used for estimating the IGS GIMs. The middle day is assumed as the target day in this process. Thirteen equally spaced time intervals are normally used for representing the VTEC. The single layer model concept which basically ignores the vertical gradient of the electron density is the basic concept in the modeling process. It assumes that all free electrons are concentrated in an infinitesimally thin layer at a fixed height (Schaer 1999). The IGS tracking network includes about 384 GNSS stations around the world. These stations are not homogeneously distributed around the world. The large gaps of this network in Middle East, *e.g.*, Iran plateau, reduce the accuracy of the IGS GIMs in these areas. Moreover, the current time delay in the delivery of these products limits their application to post-mission ones.

Empirical ionosphere models, such as international reference ionosphere (IRI), describe monthly averages of ionospheric densities and temperatures in the altitude range of 50-1500 km in the non-auroral ionosphere (Bilitza and Reinisch 2008). Beside the ground-based and satellite observations, one of the most important data sources for the IRI electron density is the worldwide network of ionosonde stations that monitor the ionosphere with varying station density. In the region with sparse ionosonde coverage, the IRI predic-

tions are less accurate. As a result, this group of ionosphere models provides coarse forecasts of VTEC values.

In this paper, a VTEC map is produced from the combination of the IRI VTEC forecasts and the Iranian Permanent GPS Network (IPGN) data in order to overcome the low accuracy of the IRI model and the IGS GIMs in Iran. Application of global support functions, such as the spherical harmonic functions, to the ionosphere modeling has been reported in several researches (Schaer 1999, Liu and Gao 2003). Spherical harmonics are global support functions. Furthermore, their efficient application requires regularly distributed data on the globe. On the other hand, to account for the small variations in the ionosphere, increasing the order and the degree of spherical harmonics is inevitable. This reduces the computational efficiency, especially for real time applications; due to the large size of observation equations involved in the problem. The bias introduced through the data cut-off at the boundaries (Gibbs phenomenon) is another deficit to the regional modeling of ionosphere using global support functions (Mautz *et al.* 2005, Schmidt 2007). Due to the disadvantages mentioned above, this paper analyzes the efficiency of the application of compactly supported base functions for representing regional VTEC values. The compactly supported base functions, such as bounded wavelets, are zero valued functions outside a bounded region (Mautz *et al.* 2005). The intensity of the solar activity, which dominates the spatial and temporal distribution of the electron density, is not uniform in the course of time. Therefore, wavelets are an appropriate mathematical tool for analyzing such non-stationary signals (Boggess and Narcowich 2009). Moreover, these base functions provide the possibility of a multi-resolution representation (Zeilhofer 2008). The presented VTEC model consists of a given reference part from IRI 2007 model and an unknown correction term. The correction term is estimated using a three-dimensional approach. Due to the localizing feature of the B-spline functions, Euclidean quadratic B-splines as compactly supported base functions with tensor-products (Stollnitz *et al.* 1995a, b, Lyche and Schumaker 2000, Schmidt 2007, Schmidt *et al.* 2008, Zeilhofer *et al.* 2009, Schmidt *et al.* 2011) are used to expand the correction term with respect to longitude, latitude and time. In this research, the VTEC from modeling, Bernese GPS software, IRI and IGS GIMs are compared with the observed VTEC derived from GPS dual-frequency observations to evaluate the accuracy of the proposed model.

2. INPUT DATA

Dual-frequency code dependent GPS receivers provide both *P*-code and beat phase pseudo-range observations on L_1 and L_2 carriers with $f_1 = 1575.42$ MHz and $f_2 = 1227.60$ MHz frequencies, respectively (Seeber

2003). The observation equations for the *P*-code and carrier phase pseudo-ranges on L_1 and L_2 frequencies are written as follows:

$$P_1 = \rho + c\left(dt - dT\right) + c\left(\tau_{P_1}^s + \tau_{P_1}^r\right) + I_1 + d_{\text{trop}} + \varepsilon_{P_1} \ , \tag{1}$$

$$P_2 = \rho + c\left(dt - dT\right) + c\left(\tau_{P_2}^s + \tau_{P_2}^r\right) + I_2 + d_{\text{trop}} + \varepsilon_{P_2} \ , \tag{2}$$

$$\Phi_1 = \rho + c\left(dt - dT\right) + c\left(\mathrm{T}_{L_1}^s + \mathrm{T}_{L_1}^r\right) + \lambda_1 N_1 - I_1 + d_{\text{trop}} + \varepsilon_{L_1} \ , \tag{3}$$

$$\Phi_2 = \rho + c\left(dt - dT\right) + c\left(\mathrm{T}_{L_2}^s + \mathrm{T}_{L_2}^r\right) + \lambda_2 N_2 - I_2 + d_{\text{trop}} + \varepsilon_{L_2} \ , \tag{4}$$

$$I_i = \frac{40.3}{f_i^2}\,\text{STEC} \ , \tag{5}$$

where P_1, P_2, Φ_1, and Φ_2 are the code and carrier phase pseudo-ranges on L_1 and L_2 signals, respectively; ρ is the geometric range from the receiver to the satellite; c is the speed of light; dt and dT are the offsets of the satellite and receiver clocks from GPS time; frequency dependent terms τ^s, τ^r, T^s, and T^r which are due to the satellite and receiver hardware delays are known as code and carrier phase inter-frequency biases; λ_1 and λ_2 are the wavelengths of the L_1 and L_2 carriers; N_1 and N_2 are carrier phase ambiguity in L_1 and L_2; I_1 and I_2 are ionospheric delays on L_1 and L_2; d_{trop} is the troposphere delay; ε_P and ε_L represent the effect of multipath and measurement noise on code and carrier phase, respectively. STEC is slant total electron content along the line of sight from satellite to receiver.

The geometry-free linear combination of GPS observations, also known as the ionospheric observable, is the subtraction of the simultaneous code or carrier phase pseudo-ranges. In this linear combination of code and carrier phase measurements, all biases except for the frequency-dependent ones are removed (Ciraolo *et al.* 2007):

$$P_4 = P_1 - P_2 = I_1 - I_2 + c\left(\tau_{P_1}^r - \tau_{P_2}^r\right) + c\left(\tau_{P_1}^s - \tau_{P_2}^s\right) + \varepsilon_P \ , \tag{6a}$$

$$P_4 = 40.3\,\text{STEC}\left(\frac{f_2^2 - f_1^2}{f_1^2 f_2^2}\right) + br + bs + \varepsilon_P \ . \tag{6b}$$

In Eqs. (6a) and (6b), $br = c(\tau_{P_1}^r - \tau_{P_2}^r)$ and $bs = c(\tau_{P_1}^s - \tau_{P_2}^s)$ are the receiver and the satellite differential inter-frequency biases on code, respectively.

$$\Phi_4 = \Phi_1 - \Phi_2 = I_2 - I_1 + \lambda_1 N_1 - \lambda_2 N_2 + c\left(\mathrm{T}_{L_1}^r - \mathrm{T}_{L_2}^r\right) + c\left(\mathrm{T}_{L_1}^s - \mathrm{T}_{L_2}^s\right) + \varepsilon_L \ , \tag{7a}$$

$$\Phi_4 = -40.3\,\mathrm{STEC}\left(\frac{f_2^2 - f_1^2}{f_1^2 f_2^2}\right) + \lambda_1 N_1 - \lambda_2 N_2 + Br + Bs + \varepsilon_L \ . \qquad (7b)$$

In Eqs. (7a) and (7b), $Br = c(\mathrm{T}^r_{L_1} - \mathrm{T}^r_{L_2})$ and $Bs = c(\mathrm{T}^s_{L_1} - \mathrm{T}^s_{L_2})$ are the receiver and the satellite differential inter-frequency biases on carrier phase, respectively.

STEC is the input data in the modeling process. This parameter is computed from the geometry-free linear combination of the code and carrier phase pseudo-ranges (see Eqs. (6) and (7)). The precision of carrier phase pseudo-ranges is much higher than the code ones. Nevertheless, carrier phase derived STEC depends on the ambiguity parameter which is not *a priori* known. In order to benefit from the ambiguity independent estimates of STEC derived from the code pseudo-ranges as well as the high precision of carrier phase measurements, code pseudo-ranges are smoothed using "carrier to code leveling process" (Ciraolo *et al.* 2007, Nohutcu *et al.* 2010).

This process benefits from the daily to monthly stability of the inter-frequency biases for receivers and satellites such that the differential inter-frequency biases in Eqs. (6) and (7) can be treated as constant parameters (Gao *et al.* 1994). Moreover, in the absence of cycle slips, the ambiguity terms in Eq. (7) can also be treated as constant parameters. Having defined a continuous arc as a group of consecutive observations in which the ambiguity parameters in the L_1 and L_2 frequencies do not change, the average of the sum of Eqs. (6) and (7) can be simplified as follows for simultaneous measurements in a continuous arc:

$$\left\langle P_4 + \Phi_4 \right\rangle_{\mathrm{arc}} = \frac{1}{n}\sum_{i=1}^{n}\left(P_4 + \Phi_4\right)_i = \left\langle \lambda_1 N_1 - \lambda_2 N_2 \right\rangle_{\mathrm{arc}} + Br + Bs + br + bs + \left\langle \varepsilon_P \right\rangle_{\mathrm{arc}} . \qquad (8)$$

In this equation, n is the number of continuous measurements contained in the arc. Subtracting Eq. (7) from Eq. (8), the ambiguity term is removed:

$$\tilde{P}_4 = \left\langle P_4 + \Phi_4 \right\rangle_{\mathrm{arc}} - \Phi_4 \approx I_1 - I_2 + br + bs + \left\langle \varepsilon_P \right\rangle_{\mathrm{arc}} - \varepsilon_L \ . \qquad (9)$$

The resulting observable, $\tilde{P}_4$ in Eq. (9), is a code ionospheric observable smoothed with the carrier phase ionospheric one. Substituting Eq. (5) into Eq. (9) results in the following linear combination in which the parameter STEC is expressed in TECU (1 TECU = 10^{16} el/m^2).

$$\tilde{P}_4 = \mathrm{STEC}\ 40.3\left(\frac{f_2^2 - f_1^2}{f_1^2 f_2^2}\right) + br + bs + \left\langle \varepsilon_P \right\rangle_{\mathrm{arc}} - \varepsilon_L \ , \qquad (10a)$$

$$\mathrm{STEC} = \left(\tilde{P}_4 - br - bs - \left\langle \varepsilon_P \right\rangle_{\mathrm{arc}} + \varepsilon_L\right)\frac{f_1^2 f_2^2}{40.3(f_2^2 - f_1^2)} \ . \qquad (10b)$$

Receiver and satellite differential code pseudo-range inter-frequency biases in Eq. (10) are known as differential code biases (DCBs). The computed STEC are usually mapped into VTEC using a mapping function (*mf*). The following function is normally used for this purpose:

$$mf = \frac{\mathrm{STEC}}{\mathrm{VTEC}} = \frac{1}{\cos z'} \quad \text{or} \quad \mathrm{VTEC} = (mf)^{-1}\mathrm{STEC} \ . \tag{11}$$

In Eq. (11), z' is the zenith angles of the satellite at the ionospheric pierce point, the intersection point of the receiver-to-satellite line of sight with the layer representing the ionosphere in the model (Schaer 1999).

3. METHOD

In this study, VTEC is decomposed into a known reference and an unknown correction term. The known reference part is computed from the IRI model. Due to the localizing feature of the B-spline functions, Euclidean quadratic B-splines and tensor-products are used for modeling the correction term. Space-time estimates of the correction term are computed using a three-dimensional approach which is based on the single layer concept.

3.1 B-spline scaling function

Let f be a signal from a certain approximation subspace $V_J \subset L_2(\mathbb{R})$, where $L_2(\mathbb{R})$ is the space of square integrable functions on real sequences. This signal is to be decomposed into a high- and a low-frequency part. The low-frequency part is obtained by an orthogonal projection of the signal into a smaller subspace $V_{J-1} \subset V_J$, which contains only the smooth functions of V_J. The orthogonal complement of V_{J-1} in V_J will be denoted by W_{J-1} (Keller 2004). The base functions for spaces V_J and W_J are known as scaling functions and wavelets of level J, respectively. These two functions generate a family of functions that can be used for decomposing (analyzing) or reconstructing (synthesis) the signal.

A special kind of wavelets is generated by B-splines, offering useful properties, such as compact support, semi-orthogonality, symmetry and simplicity. The polynomial B-splines on a bounded interval has been introduced by Chui and Quak (1992), whereas the decomposition and reconstruction algorithms are presented in Quak and Weyrich (1994). User friendly algorithms and their application can be found in Stollnitz *et al*. (1995a, b).

Normalized B-spline scaling functions $\phi_{J,k}(x) = N^d_{J,k}(x)$ of degree d, resolution level J, shift k and variable x are recursively defined by Eq. (12), with the initial values of Eq. (13). When the denominators of Eq. (12) are zero, the fractions are set to zero (Stollnitz *et al.* 1995a, b). Scaling functions

space V_J has $K_J = 2^J + d$ base functions (the function space dimension), $t_0, t_1, \ldots, t_{K_J+d}$ is a sequence of non-decreasing equally spaced values called knots and $k = 0, 1, \ldots, K_J - 1$ are shift values for each scaling function. Increasing the level of the scaling function, the function becomes narrower and consequently more details of the analyzing signal can be modeled.

$$\phi_{J,k}(x) = N_{J,k}^{d}(x) = \frac{x - t_k^J}{t_{k+d}^J - t_k^J} N_{J,k}^{d-1}(x) + \frac{t_{k+d+1}^J - x}{t_{k+d+1}^J - t_{k+1}^J} N_{J,k+1}^{d-1}(x) \ , \tag{12}$$

$$N_{J,k}^{0}(x) = \begin{cases} 1 & \text{if} \quad t_k^J \le x < t_{k+1}^J \\ 0 & \text{otherwise} \end{cases} . \tag{13}$$

In regional modeling of ionosphere, endpoint-interpolating B-spline on unit interval $[0, 1]$ is used to avoid the edge effect at the boundaries; for this purpose the first $d + 1$ knots are set to zero and the last $d + 1$ knots are set to one – see Eq. (14) (Mautz *et al.* 2005, Schmidt 2007, Zeilhofer 2008).

$$\left(t_0, t_1, \ldots, t_{K_J+d}\right) = \frac{1}{2^J}\left(\underbrace{0, \cdots, 0}_{d+1 \text{ times}}, 1, 2, \cdots, 2^J - 1, \underbrace{2^J, \cdots, 2^J}_{d+1 \text{ times}}\right) . \tag{14}$$

3.2 Ionosphere modeling

In this study, based on the single layer concept, a three dimensional approach is used for modeling the VTEC in space-time domains. B-splines are used as the base functions in the model. The model is developed in a geocentric Earth-fixed coordinate system and the time variation of VTEC is accounted for by using the code and carrier phase measurements of the IPGN as well as the IRI forecasts of VTEC.

The VTEC(λ, φ, t) computed from GPS measurements, Eqs. (10) and (11), is decomposed into a reference or approximate part VTEC$_{\text{ref}}(\lambda, \varphi, t)$ extracted from IRI and a correction term ΔVTEC(λ, φ, t) – see Eq. (15), to be estimated:

$$\text{VTEC}(\lambda, \varphi, t) = \text{VTEC}_{\text{ref}}(\lambda, \varphi, t) + \Delta\text{VTEC}(\lambda, \varphi, t) \ . \tag{15}$$

The correction term ΔVTEC(λ, φ, t) is expanded into three-dimensional B-spline scaling functions $\phi_{J_1 J_2 J_3, k_1 k_2 k_3}(\lambda, \varphi, t)$ with the unknown scaling coefficients $d_{J_1 J_2 J_3, k_1 k_2 k_3}$:

$$\Delta\text{VTEC}(\lambda, \varphi, t) = \sum_{k_1=0}^{K_{J_1}-1} \sum_{k_2=0}^{K_{J_2}-1} \sum_{k_3=0}^{K_{J_3}-1} d_{J_1 J_2 J_3, k_1 k_2 k_3} \phi_{J_1 J_2 J_3, k_1 k_2 k_3}(\lambda, \varphi, t) \ . \tag{16}$$

Applying tensor product to the three-dimensional B-spline scaling functions $\phi_{J_1J_2J_3,k_1k_2k_3}(\lambda,\varphi,t)$ of levels J_1, J_2, and J_3 w.r.t. λ, φ, and t, these functions are reduced into the product of three one-dimensional scaling functions $\varphi_{J,k}(x)$ of levels $J \in \{J_1, J_2, J_3\}$, shift $k \in \{k_1, k_2, k_3\}$ and variable $x \in \{\lambda, \varphi, t\}$:

$$\phi_{J_1J_2J_3,k_1k_2k_3}(\lambda,\varphi,t) = \phi_{J_1,k_1}(\lambda)\,\phi_{J_2,k_2}(\varphi)\,\phi_{J_3,k_3}(t)\ . \tag{17}$$

One-dimensional normalized quadratic scaling functions computed using the algorithm introduced in the previous section are used instead of the B-spline scaling functions $\varphi_{J,k}(x)$ in Eq. (17). Since the variable x in scaling function $\varphi_{J,k}(x)$ takes value on the unit interval [0, 1], variables λ, φ, and t are transformed to this interval using the following equation:

$$x = \frac{\lambda - \lambda_{\min}}{\lambda_{\max} - \lambda_{\min}}, \quad y = \frac{\varphi - \varphi_{\min}}{\varphi_{\max} - \varphi_{\min}}, \quad z = \frac{t - t_{\min}}{t_{\max} - t_{\min}}, \tag{18}$$

in which the quantities $\lambda_{\min}$, $\lambda_{\max}$, $\varphi_{\min}$, and $\varphi_{\max}$ are the boundary coordinates of modeling area and $t_{\min}$ and $t_{\max}$ are the starting and ending epochs of the modeling interval. Substituting Eq. (17) into Eq. (16) and considering Eq. (18), the correction term is re-written as follows:

$$\Delta\mathrm{VTEC}(x,y,z) = \sum_{k_1=0}^{K_{J_1}-1}\sum_{k_2=0}^{K_{J_2}-1}\sum_{k_3=0}^{K_{J_3}-1} d_{J_1J_2J_3,k_1k_2k_3}\,\phi_{J_1,k_1}(x)\,\phi_{J_2,k_2}(y)\,\phi_{J_3,k_3}(z)\,. \tag{19}$$

The simultaneous system of observation equations required for computing the unknown coefficients $d_{J_1J_2J_3,k_1k_2k_3}$ constructed from Eqs. (10), (11), (15), and (19) can be written in the following form:

$$\mathbf{A}\mathbf{x} = \mathbf{b} + \mathbf{r}\ , \tag{20}$$

in which **b** is the vector of observations or the correction term ($b_i = \Delta\mathrm{VTEC}_i = \mathrm{VTEC}_i - \mathrm{VTEC}_{\mathrm{ref}\,i}$), **r** is the vector of residual, **A** is the coefficient or design matrix comprising scaling function values which describes the relations between observations and model parameters, **x** is the model parameter vector including unknown scaling coefficients $(d_{J_1J_2J_3,k_1k_2k_3})$. The correction term and scaling function values are computed at each epoch for every observation point. The satellite and receiver differential code biases (in Eq. (10)) are considered as known quantities. The satellite DCBs are the IGS products and the receiver DCBs are computed in preprocessing step.

Since B-spline scaling functions are local support in nature, the unknown parameters in the simultaneous observation equations, Eq. (20), are not completely constrained with irregularly distributed data (see the ionospheric observables in Fig. 1). As a result, the coefficient matrix **A** is a sparse matrix.

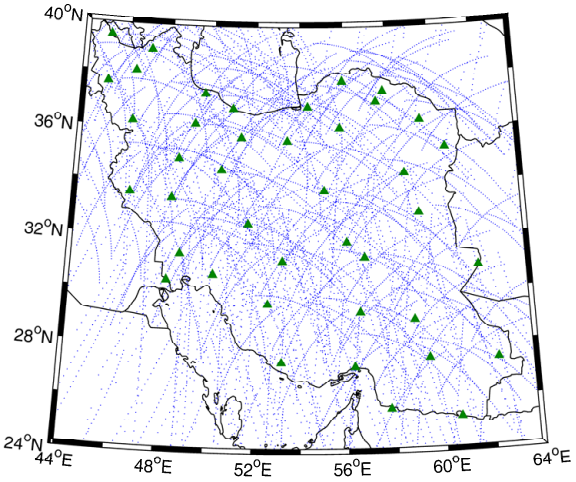

Fig. 1. Distribution of the GPS stations (triangles) and ionospheric observables (dots) in modeling area.

Using the geometric theorem of singular value decomposition, the design matrix can be expressed in its spectral form (Hansen 1997). When the singular values of the coefficient matrix in a simultaneous system of equations decay asymptotically to zero, the problem is probably ill-conditioned. To analyze the conditioning of the problem in further detail, the discrete Picard condition can be used (Hansen 1990), Picard condition can also be used for analyzing the instability of the least-squares solution to Eq. (20) (*e.g.*, Hossainali 2006, p. 57-58).

Depending on the modeling time interval and the scaling function level used in the modeling process, the size of coefficient matrix may become very large. This increases the number of unknown parameters. When the coefficient matrix is large, iterative regularization techniques are normally preferred to the direct ones. The least-squares QR (LSQR) is one of the iterative regularization methods which is based on Lanczos bidiagonalization and QR factorization. The method numerically provides a more reliable solution for a large, sparse and ill-conditioned system of simultaneous equations as compared to the direct techniques (Paige and Saunders 1982). LSQR is one of the Krylov subspace iterative methods. Due to the semi-convergence property of LSQR, the L-curve method is used to determine the regularization parameter or the step at which the iteration process should stop (Hansen 1994). The iteration number is selected as the closest point to the corner of this curve.

4. RESULTS

In this study, dual-frequency GPS code and carrier phase measurements of 41 GPS permanent stations from the IPGN has been used for three-

dimensional modeling of the ionosphere in Iran. The sampling rate of the measurements is 30 s and the observation epoch is 3 January 2007. Figure 1 illustrates the spatial distribution of the GPS stations (triangles) and ionospheric observables (dots).

The height of the single layer model used for modeling the spatial variation of the ionosphere is taken to be 450 km. The adopted elevation cut-off angle for the observations is taken to be 15 degrees. According to the K_P index values (an indication for geomagnetic activity of the Earth) reported by the International Service for Geomagnetic Indices, the maximum electron density and therefore VTEC is expected to occur from $t = 5$ to 15 UT. The IRI an GPS data of two successive hours are used for estimating the VTEC map. Usually the middle hour is assumed as the target hour in this process. For example, to model the VTEC at epoch $t = 14$ UT, the IRI and GPS measurements of the time interval 13 to 15 UT are used. In order to validate the accuracy of VTEC model and to come up with an optimum level for the computed three-dimensional model, the correction term has been expanded at seven different levels of: $J_1 = J_2 = J_3 = 1$, $J_1 = J_2 = J_3 = 2$, $J_1 = J_2 = J_3 = 3$, $J_1 = J_2 = 3$, $J_3 = 4$, $J_1 = J_3 = 3$, $J_2 = 4$, $J_1 = 4$, $J_2 = J_3 = 3$, and $J_1 = J_2 = J_3 = 4$. Table 1 summarizes the root mean square (RMS) of residuals and the number of unknown coefficients in each level. This information is given for five different epochs. To compare various levels together, the mean values of the RMS are also reported.

Table 1

RMS of residuals and coefficients number

Level	RMS [TECU]						Coefficients number
	UT = 06	UT = 08	UT = 10	UT = 12	UT = 14	Mean	
111	0.77	0.79	0.74	0.86	0.68	0.77	64
222	0.72	0.77	0.71	0.84	0.65	0.74	216
333	0.66	0.71	0.68	0.79	0.62	0.69	1000
334	0.65	0.70	0.67	0.77	0.61	0.68	1800
343	0.60	0.65	0.61	0.72	0.57	0.63	1800
433	0.59	0.63	0.62	0.71	0.55	0.62	1800
444	0.42	0.50	0.49	0.63	0.41	0.49	5832

The Bernese GPS Software V5.0 which uses spherical harmonics for VTEC modeling (Dach *et al.* 2007) also has been used to produce VTEC maps in Iran. Spherical harmonics of the degree and order $n = 5$, $m = 5$, as suggested by the Bernese software developing team, has been taken into account. Figure 2 shows the Bernese VTEC map at epoch $t = 14$ UT.

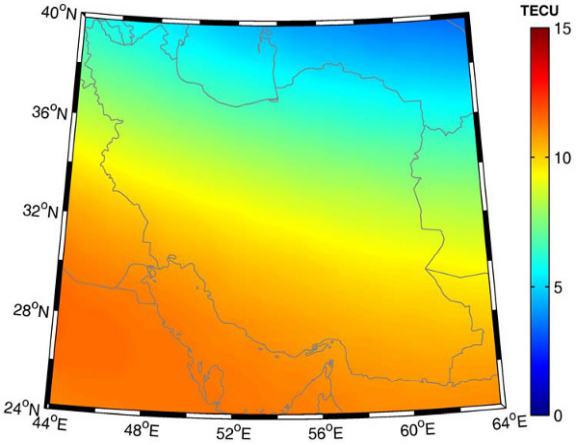

Fig. 2. Bernese VTEC map for $n = 5$, $m = 5$. Colour version of this figure is available in electronic edition only.

In order to evaluate the accuracy of the VTEC estimation, some of observed VTEC (derived from GPS dual-frequency observations) at each GPS station are excluded from the modeling process. The observed VTEC are finally compared with estimated value. The difference between the observed and estimated VTEC is referred to as the "VTEC estimation error". VTEC obtained from the Bernese GPS software, IRI and IGS GIMs are also compared with the observed VTEC. Table 2 summarizes the RMS of VTEC es-

Table 2

VTEC estimation error statistics at TEHN station

Method	UT = 06		UT = 08		UT = 10		UT = 12		UT = 14		Mean	
	RMS	RE	RMS	RE	RMS	RE	RMS	RE	RMS	RE	RMS	RE
111	0.58	3.94	0.73	5.36	0.47	4.30	0.50	3.65	0.45	4.71	0.55	4.39
222	0.49	3.20	0.67	4.78	0.46	4.33	0.48	3.62	0.47	4.81	0.51	4.15
333	0.46	2.77	0.63	4.35	0.45	4.18	0.45	3.54	0.46	5.08	0.49	3.98
334	0.46	2.79	0.62	4.28	0.47	4.37	0.44	3.43	0.46	5.06	0.49	3.99
343	0.42	2.43	0.64	4.36	0.43	3.86	0.45	3.37	0.42	4.54	0.47	3.71
433	0.43	2.44	0.62	4.37	0.49	4.40	0.50	3.90	0.44	4.60	0.50	3.94
444	0.39	2.04	0.57	4.00	0.45	3.75	0.49	3.92	0.44	3.95	0.47	3.53
Bernese	1.88	12.13	1.86	13.23	1.03	8.88	0.80	6.30	0.76	7.00	1.27	9.51
IRI	3.61	22.06	2.54	16.50	1.80	16.89	1.99	18.10	3.76	47.04	2.74	24.12
CODE	3.56	29.11	4.18	36.24	4.37	47.33	4.01	44.99	3.43	47.92	3.91	41.12
ESA	3.67	30.15	4.36	37.91	4.83	52.86	4.40	49.77	3.88	54.16	4.23	44.97
JPL	5.13	42.82	6.40	56.95	5.65	61.53	4.99	56.43	4.94	68.56	5.42	57.26
UPC	2.84	23.02	3.85	33.05	4.46	48.63	3.48	38.92	2.88	40.01	3.50	36.73
IGS	3.78	31.16	4.66	40.80	4.82	52.50	4.20	47.44	3.74	52.32	4.24	44.84

timation error (in TECU) and their mean relative error (RE) (in percent) at station Tehran. Computations are reported for five different epochs. To compare various methods together, the means of the RMS and RE are also reported.

Comparing the RMS of VTEC estimation error (reported for seven levels) to the RMS of the Bernese VTEC error confirms the efficiency of the compactly supported base functions for regional modeling of VTEC. Moreover, comparing the RMS of VTEC estimation error to the RMS of the IRI and IGS GIMs VTEC error also indicates the superiority of the proposed method for ionosphere modeling in the region with large gaps of IRI ionosonde and IGS network stations.

The RMS of residuals indicate how the model fits the observations. By increasing the level of space function to 3, the RMS of residuals and the RMS of VTEC estimation error decrease. From level 4, the oscillation of model increases between the observations and therefore, RMS of VTEC estimation error are not considerably improved. Moreover, increasing the level of space function, increases the number of unknown coefficients and reduces the computational efficiency of the modeling process, especially for real-time or near-real-time applications. Hence, computational level $J_1=J_2=J_3=3$, could be the optimum level for regional modeling of VTEC. Nevertheless, each level can be selected according to the application precision and computation burden. Relative error of this level indicates that the estimated VTEC can recover about 96% of VTEC in ionosphere.

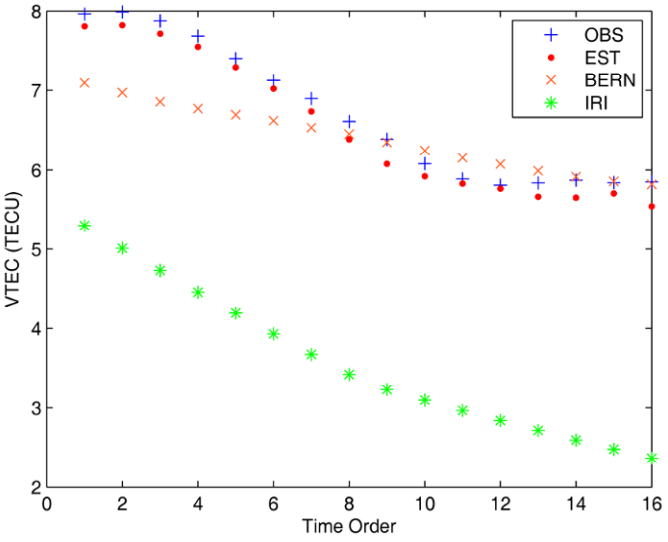

Fig. 3. Observed, estimated, Bernese, and IRI VTEC for PRN 15 at TEHN station. Colour version of this figure is available in electronic edition only.

Observed, level 3 estimated, Bernese and IRI VTEC at epoch $t = 14$ UT for PRN 15 at station TEHN are shown in Fig. 3. RMS of VTEC estimation error is 0.18 TECU, RMS of Bernese VTEC error is 0.55 TECU and RMS of IRI VTEC error is 3.14 TECU. Estimated VTECs closely approximate the observed one. Bernese VTECs approximate the trend of observations which

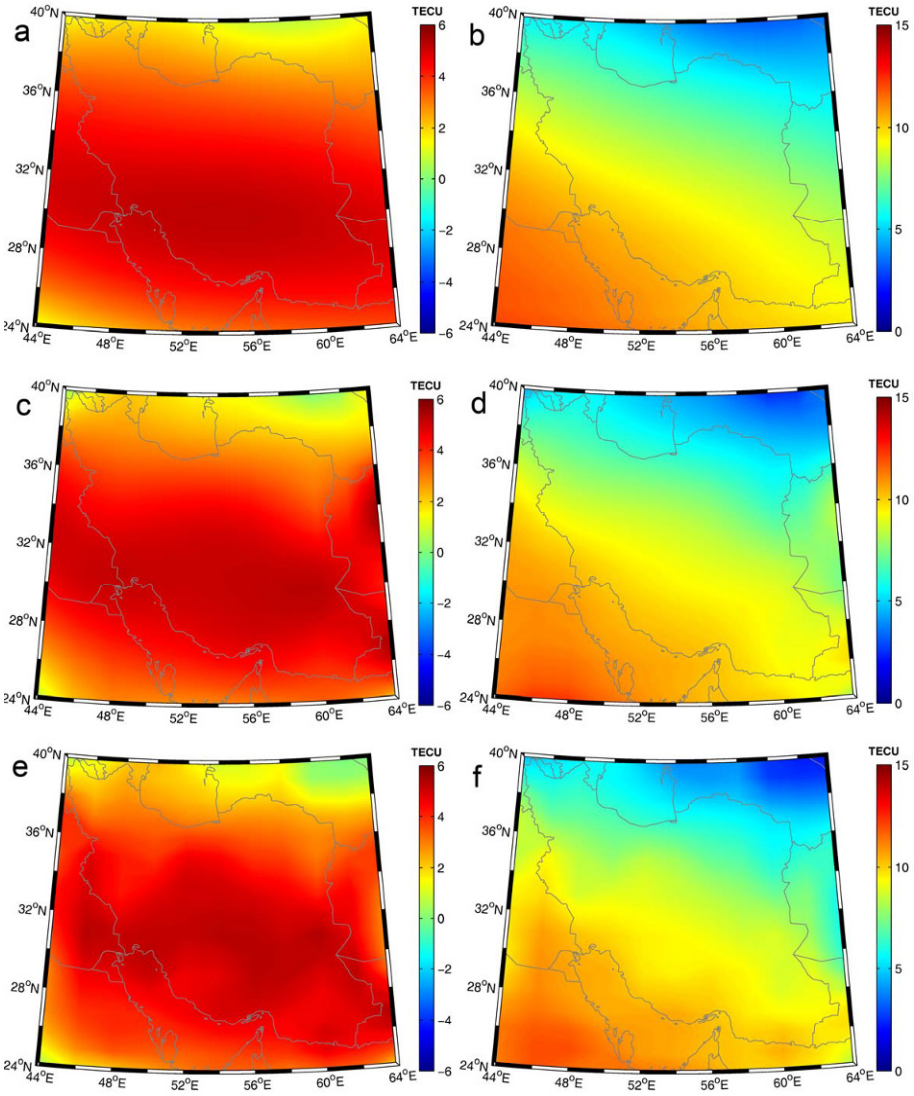

Fig. 4. VTEC estimation at time $t = 14$ UT: (a) correction term, (b) VTEC map for $J_1 = J_2 = J_3 = 1$, (c) correction term, (d) VTEC map for $J_1 = J_2 = J_3 = 2$, (e) correction term, and (f) VTEC map for $J_1 = J_2 = J_3 = 3$. Colour version of this figure is available in electronic edition only.

is expected from spherical harmonic functions. This confirms the capability of spherical harmonic functions for modeling the long term variations of VTEC. IRI VTEC have large disagreement with observed VTECs. VTEC extracted from the ISG GIMs also show a large disagreement with the observed VTEC (RMS of CODE VTEC error is 3.92 TECU, RMS of ESA VTEC error is 4.36 TECU, RMS of JPL VTEC error is 5.18 TECU, RMS of UPC VTEC error is 3.31 TECU, and RMS of IGS combined VTEC error is 4.17 TECU).

Figure 4 shows the correction term and VTEC map for first three levels at epoch $t = 14$ UT. Using the L-curve method, evaluated unknown coefficients at iteration 12 of 1000 were selected for level 3 solution.

5. CONCLUSIONS

This paper presents regional VTEC model based on the IRI 2007 and GPS observations from Iranian Permanent GPS Network. The VTEC is decomposed into a known reference and an unknown correction term. The reference part is taken from the IRI 2007 model. Due to the localizing feature of B-spline functions, a three-dimensional approach based on Euclidean quadratic B-splines and tensor-products is used to model the correction term. The LSQR iterative regularization method, which is numerically reliable in large, sparse and ill-posed system, with the L-curve method to determine the stopping iteration number, is used for estimating the unknown parameter. This is the first paper in which the IRI extracted VTEC are improved regionally by compactly supported base functions using GPS observations and its accuracy are assessed by observed VTEC derived from GPS dual-frequency observations. The RMS of VTEC estimation error is about 0.50 TECU and RMS of the Bernese VTEC error is about 1.27 TECU. This difference confirms the superiority of the compactly supported base functions for regional modeling of VTEC. The large disagreement between the RMS of VTEC estimation error with RMS of IRI VTEC error (2.74 TECU), RMS of CODE VTEC error (3.91 TECU), RMS of ESA VTEC error (4.23 TECU), RMS of JPL VTEC error (5.42 TECU), RMS of UPC VTEC error (3.5 TECU), and RMS of IGS combined VTEC error (4.24 TECU) indicates the efficiency of the proposed method for ionosphere modeling in the region with large gaps of IRI ionosonde and IGS network stations.

Acknowledgment. Authors would like to thank the National Cartographic Center of Iran (NCC) for providing GPS data. Reviewers are acknowledged for their constructive comments.

References

Bilitza, D., and B.W. Reinisch (2008), International Reference Ionosphere 2007: Improvements and new parameters, *Adv. Space Res.* **42**, 4, 599-609, DOI: 10.1016/j.asr.2007.07.048.

Boggess, A., and F.J. Narcowich (2009), *A First Course in Wavelets with Fourier Analysis*, 2nd ed., John Wiley & Sons, Hoboken, 315 pp.

Chui, C.K., and E. Quak (1992), Wavelets on a bounded interval. **In:** D. Braess and L.L. Schumaker (eds.), *Numerical Methods of Approximation Theory*, Vol. 9, International Series of Numerical Mathematics 105, Birkhauser Verlag, Basel, 53-75, DOI: 10.1007/978-3-0348-8619-2_4.

Ciraolo, L., F. Azpilicueta, C. Brunini, A. Meza, and S.M. Radicella (2007), Calibration errors on experimental slant total electron content (TEC) determined with GPS, *J. Geod.* **81**, 2, 111-120, DOI: 10.1007/s00190-006-0093-1.

Dach, R., U. Hugentobler, P. Fridez, and M. Meindl (eds.) (2007), *Bernese GPS Software Version 5.0*, Astronomical Institute, University of Bern, Bern, Switzerland.

Gao, Y., P. Heroux, and J. Kouba (1994), Estimation of GPS receiver and satellite L1/L2 signal delay biases using data from CACS. **In:** *Proc. KIS-94, 30 August – 2 September 1994, Banff, Canada*, 109-117.

Hansen, P.C. (1990), The discrete Picard condition for discrete ill-posed problems, *BIT* **30**, 4, 658-672, DOI: 10.1007/BF01933214.

Hansen, P.C. (1994), Regularization tools: a Matlab package for analysis and solution of discrete ill-posed problems, *Numer. Algorithms* **6**, 1, 1-35, DOI: 10.1007/BF02149761.

Hansen, P.C. (1997), *Rank-deficient and Discrete Ill-posed Problems. Numerical Aspects of Linear Inversion*, Monographs on Mathematical Modeling and computation, Vol. 4, SIAM, Philadelphia.

Hernández-Pajares, M., J.M. Juan, and J. Sanz (1999), New approaches in global ionospheric determination using ground GPS data, *J. Atmos. Sol.-Terr. Phys.* **61**, 16, 1237-1247, DOI: 10.1016/S1364-6826(99)00054-1.

Hernández-Pajares, M., J.M. Juan, J. Sanz, R. Orus, A. García-Rigo, J. Feltens, A. Komjathy, S.C. Schaer, and A. Krankowski (2009), The IGS VTEC maps: a reliable source of ionospheric information since 1998, *J. Geod.* **83**, 3-4, 263-275, DOI: 10.1007/s00190-008-0266-1.

Hossainali, M.M. (2006), A comprehensive approach to the analysis of the 3D-kinematics of deformation, Ph.D. Thesis, Institute of Physical Geodesy, Darmstadt University of Technology, Darmstadt, Germany, 152 pp.

Keller, W. (2004), *Wavelets in Geodesy and Geodynamics*, Walter de Gruyter GmbH & Co. KG, Berlin.

Liu, Z., and Y. Gao (2003), Ionospheric TEC predictions over a local area GPS reference network, *GPS Solut.* **8**, 1, 23-29, DOI: 10.1007/s10291-004-0082-x.

Lyche, T., and L.L. Schumaker (2000), A multiresolution tensor spline method for fitting functions on the sphere, *SIAM J. Sci. Comput.* **22**, 2, 724-746, DOI: 10.1137/S1064827598344388.

Mautz, R., J. Ping, K. Heki, B. Schaffrin, C. Shum, and L. Potts (2005), Efficient spatial and temporal representations of global ionosphere maps over Japan using B-spline wavelets, *J. Geod.* **78**, 11-12, 660-667, DOI: 10.1007/s00190-004-0432-z.

Nohutcu, M., M.O. Karslioglu, and M. Schmidt (2010), B-spline modeling of VTEC over Turkey using GPS observations, *J. Atmos. Sol.-Terr. Phys.* **72**, 7-8, 617-624, DOI: 10.1016/j.jastp.2010.02.022.

Paige, C.C., and M.A. Saunders (1982), LSQR: an algorithm for sparse linear equations and sparse least squares, *ACM Trans. Math. Softw.* **8**, 1, 43-71, DOI: 10.1145/355984.355989.

Quak, E., and N. Weyrich (1994), Decomposition and reconstruction algorithms for spline wavelets on a bounded interval, *Appl. Comput. Harmon. Anal.* **1**, 3, 217-231, DOI: 10.1006/acha.1994.1009.

Schaer, S. (1999), Mapping and predicting the Earth's ionosphere using the Global Positioning System, Ph.D. Thesis, Astronomical Institute, University of Bern, Bern, Switzerland.

Schmidt, M. (2007), Wavelet modeling in support of IRI, *Adv. Space Res.* **39**, 5, 932-940, DOI: 10.1016/j.asr.2006.09.030.

Schmidt, M., D. Bilitza, C.K. Shum, and C. Zeilhofer (2008), Regional 4-D modeling of the ionospheric electron density, *Adv. Space Res.* **42**, 4, 782-790, DOI: 10.1016/j.asr.2007.02.050.

Schmidt, M., D. Dettmering, M. Mößmer, Y. Wang, and J. Zhang (2011), Comparison of spherical harmonic and B spline models for the vertical total electron content, *Radio Sci.* **46**, 6, RS0D11, DOI: 10.1029/2010RS004609.

Seeber, G. (2003), *Satellite Geodesy: Foundations, Methods, and Applications*, 2nd ed., Walter de Gruyter GmbH & Co. KG, Berlin, 589 pp.

Stollnitz, E.J., T.D. Derose, and D.H. Salesin (1995a), Wavelets for computer graphics: A primer. Part 1, *IEEE Comput. Graph. Appl.* **15**, 3, 76-84, DOI: 10.1109/38.376616.

Stollnitz, E.J., T.D. Derose, and D.H. Salesin (1995b), Wavelets for computer graphics: A primer. Part 2, *IEEE Comput. Graph. Appl.* **15**, 4, 75-85, DOI: 10.1109/38.391497.

Zeilhofer, C. (2008), Multi-dimensional B-spline modeling of spatio-temporal ionospheric signals, Reihe A123, Deutsche Geodätische Kommission, München.

Zeilhofer, C., M. Schmidt, D. Bilitza, and C.K. Shum (2009), Regional 4-D modeling of the ionospheric electron density from satellite data and IRI, *Adv. Space Res.* **43**, 11, 1669-1675, DOI: 10.1016/j.asr.2008.09.033.

Received 1 April 2012
Received in revised form 24 October 2012
Accepted 28 January 2013